Hindawi
Shock and Vibration
Volume 2019, Article ID 2350675, 20 pages
https://doi.org/10.1155/2019/2350675

Research Article

Shaking Table Array Tests of an Ultra-High-Voltage Cup-Type Transmission Tower-Line System

Fei Wang,[1,2] Ke Du,[1] Jingjiang Sun,[1] Fuyun Huang,[3] and Zhenghui Xiong[3]

[1]*Key Laboratory of Earthquake Engineering and Engineering Vibration, Institute of Engineering Mechanics, China Earthquake Administration, Harbin 150080, China*
[2]*China Electric Power Research Institute, Beijing 100192, China*
[3]*College of Civil Engineering, Fuzhou University, Fuzhou 350106, China*

Correspondence should be addressed to Ke Du; duke@iem.ac.cn

Received 28 August 2019; Accepted 18 November 2019; Published 11 December 2019

Academic Editor: Rui Moreira

Ultra-high-voltage (UHV) cup-type transmission towers supported with long-span transmission lines are unavoidably subjected to the coupling action between the towers and the transmission lines. Therefore, investigating how tower-line coupling affects UHV cup-type transmission towers is important. In this study, three shaking table array tests of an UHV cup-type transmission tower-line system were carried out to investigate the dynamic characteristics of the coupling action between the towers and transmission lines based on the following four comparative models: a single-tower model, a single-tower model with suspended lumped masses, a three-tower-two-line model, and a five-tower-four-line model. The test results demonstrated that the tower-line coupling interaction had a significant effect on the dynamic characteristics and seismic responses, as the suspended conductor line and the suspended lumped mass decreased the frequency of the transmission tower. Under longitudinal ground motion, the model with the suspended lumped mass had the lowest peak acceleration response and the largest peak displacement response. Under the same ground motion, the four models had similar peak strains in the longitudinal direction. Under transverse-the-line ground motion, the model with the suspended lumped mass had the lowest peak acceleration response and the smallest peak responses for displacement and strain in the transverse direction; therefore, this model is inappropriate for the simulation and seismic evaluation of transmission tower-line systems.

1. Introduction

Electricity transmission systems consisting of transmission towers and transmission lines have been widely recognized as lifeline systems; in the system, the transmission tower is a type of lattice tower that supports the overhead transmission lines. Compared with other power equipment, the ultrahigh voltage (UHV) transmission tower structures are characterized by great heights, long spans, and complex tower-line coupling effects. However, this type of structure is generally considered to be less impacted by seismic action, and relevant studies are rare [1–4]. The mechanical performance of this type of structure under disastrous dynamic wind and ice loads is the main focus of the research performed worldwide [5–9].

However, earthquakes have frequently occurred in recent years worldwide, and the power transmission systems have been severely damaged in earthquake-ridden regions [10]. The earthquake damage investigations indicate that transmission line damage is severe [11]. As revealed by the investigations of the damage to transmission lines caused by several typical major earthquakes, seismic damage mainly manifests as tower tilting, insulator breakage, and foundation settling and dislocation. For example, in the 1994 Northridge earthquake in the United States, a few high-voltage transmission towers were damaged; the level of damage to the transmission towers was related to the intensity of the ground motion and the seismic design. In the 1995 Hanshin earthquake in Japan, 23 overhead transmission lines were damaged and 11 steel transmission

towers collapsed. During the 1999 Chi-Chi earthquake, transmission lines were severely damaged, including 28 345-kilovolt UHV transmission lines, amounting to a damage rate close to 30%. In the 2008 Wenchuan earthquake, more than 20 over-10-kilovolt transmission towers collapsed, and approximately 16 towers were locally damaged, resulting in severe damage[12]. During the 2013 Lushan earthquake in Sichuan, 265 over-10-kilovolt transmission towers with distribution lines out-of-service and 224 over-35-kilovolt lines were severely damaged, reaching a damage rate of 50% and resulting in huge losses [13]. Considering the harsh and complex geological conditions of the areas along UHV transmission lines, if one tower is damaged or collapses under a strong earthquake, the operation of the whole transmission line will be affected. Therefore, the mechanical mechanism and failure mode of transmission tower structures under strong earthquakes and the corresponding seismic theory and methods have garnered increasing amounts of attention [14, 15].

Shaking table tests can reproduce the actual stress state of a structure under an earthquake well and can be used to study the structural dynamic performance, structural response, and failure mode under seismic action. However, the UHV transmission tower-line system is characterized by tall towers (the UHV transmission towers built in China generally exceed 100 m in height) and extremely large spans (e.g., longer than 1000 m), so it is difficult to meet the experimental requirements with single shaking table test equipment. Therefore, shaking table tests of UHV transmission tower-line systems have not often been carried out as conventional civil structures. The earliest known shaking table tests of high-voltage transmission towers were conducted in the 1980s. Kotsubo et al. [16] conducted a shaking table test of three transmission towers in south eastern Kyushu, Japan. The researchers considered the influence of the conductor lines and the ground lines on the adjacent towers, obtained the dynamic characteristics of the transmission towers under earthquakes, and proposed a corresponding seismic calculation method for the transmission towers. Filiatrault [17] conducted a shaking table test of five different electrical substation equipment components, considered the interactions between the conductor lines and insulators with different degrees of relaxation under earthquakes, and concluded that the three flexible conductor lines with different degrees of relaxation had little impact on the insulators under earthquakes. Kempner et al. [18] conducted dynamic tests and theoretical analysis of the modeling of guyed towers. Tian et al. [19] considered the length limitation of the shaking table for the extremely large span of a high-voltage transmission tower-line system and noted that the tower-to-line scale factor for a high-voltage transmission tower-line system is difficult to maintain. Based on numerical analysis, those of the conductor line and ground line were corrected with the similitude ratio of the transmission tower remaining constant. Shi et al. [20] conducted a shaking table test of a simplified long-span transmission tower-line coupling system using steel rods with a diameter of 10 mm to simulate the transmission tower and a steel chain to simulate the conductor line. Three steel rods were connected by two layers of steel chains to form a transmission tower-line coupling system model. This test verified the accuracy of the proposed theoretical calculation method for the transmission line-line coupling system and reflected the dynamic characteristics of a high-voltage transmission tower-line system. However, the experimental model was overly simplified, and the chains that were used to simulate the conductor lines were relaxed and failed to truly reflect the mechanical performance of the tower structure and conductor line. Considering the deficiencies of the shaking table tests by Bai et al., [21, 22] proposed a new model design method for shaking table tests for a UHV transmission tower-line coupling system with double circuits on the same tower and geometric nonlinearity and conducted a shaking table test of a UHV grid transmission tower-line system. Aiming at a coupling system consisting of two different structural forms, i.e., a highly geometrically nonlinear conductor line and ground line and an elastic transmission tower structure, a design method for a separate model with dynamic parameters was proposed in the experimental scheme to address the problem that a tower-line system with a uniform scale cannot meet the length limitation of a shaking table. Xie et al. [23–25] conducted a number of shaking table tests of a high-voltage transmission angle-steel tower-line system and obtained the dynamic response characteristics of UHV angle steel transmission towers, the effects of the mass of the conductor line and ground line on the dynamic response of the tower structure, and the nonlinear vibration responses of the conductor line and ground line of a UHV transmission tower-line coupling system. An improved test method was proposed, and many important conclusions were drawn, which provided a reference for future shaking table tests of tower-line system models. However, most of the research results were obtained based on single shaking tables.

The above studies show that the main problem in the shaking table tests of UHV transmission tower-line systems are the length limitations of single shaking tables; the use of an array of shaking tables to capture the interactions in transmission tower-line systems is scarce, making it difficult to consider the effect of tower-line coupling on the transmission towers' responses. In this paper, an array of three shaking tables are used to test UHV cup-type transmission towers-line systems to investigate the interactions in transmission tower-line systems.

2. Model Design of the UHV Cup-Type Transmission Tower-Line System

A typical transmission tower prototype, the ZBC30102A-type self-supporting suspension tower in the Ximeng-Shandong UHV project, is chosen for the shaking table tests. The tower has a height of 73.8 m and a line span of 500 m; the prototype has three conductor lines, which are suspended in the middle and on both sides of the tower head through insulators. The conductor line and the ground line types are JL/G1A-630/45 and JLB20A-170, respectively. The transmission tower prototype is shown in Figure 1.

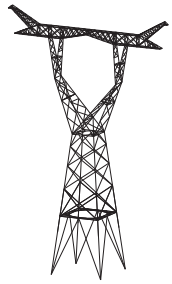

Figure 1: UHV cup-type steel tower ZBC30102A.

2.1. Design and Manufacture of the Tower

2.1.1. Geometric Similitude Ratio and Material Selection. Considering the size limitations of the shaking tables, which have side lengths of 2.5 m, the geometric similitude ratio of the transmission tower is assumed to be 1 : 15.

If all the angle steel members are scaled based on the geometric scale ratio, for the cross section, it is difficult to make the members because their thickness would only be 0.02 mm. Therefore, the transmission tower model uses four specifications of the angle steel (L30 × 3, L25 × 3, L20 × 3, and L10 × 1). The L30 angle steel is used for the main members and diagonal members of the tower leg and tower body, the L25 angle steel is used for the main members and diagonal members of the upper and lower cranks, and the L20 angle steel is used for main members and diagonal members of the ground line supports and crossarms. The auxiliary members of the model tower are made of L10 angle steel, and welded connections are used.

2.1.2. Other Similitude Coefficients. The same material is chosen to use in the towers of the experimental model as is used in the prototype; therefore, the similitude ratio for the elastic modulus E is 1 : 1, and considering the noise and bearing capacity of the shaking tables, the similitude coefficient of acceleration is assumed to be 3 : 1. Then, other similitude coefficients are derived as the preliminary similarity relationships by using dimensional analysis and based on the Buckingham π theorem for the transmission tower model design (Table 1).

The total mass of the prototype transmission tower is 83544.6 kg, and the total mass of the scaled transmission tower model is 642.65 kg.

2.1.3. The Counterweight of the Model. Because the density similitude ratio is 5 : 1, the total mass of the scaled transmission tower model is 642.65 kg, the weight of the transmission tower without a counterweight is 128.53 kg, and the mass of the actual scaled transmission tower without a counterweight is 129 kg; to evenly apply the counterweight, the actual balancing weight is 555 kg. The actual total mass of the manufactured transmission tower model is 684 kg, and the actual density similitude ratio is 5.3 : 1. In the tests, two counterweights are processed, with masses of 2 kg and 0.25 kg. The counterweights are shown in Figure 2.

Table 1: Similitude coefficients of the transmission tower model.

Physical quantity	Ratio of similitude (model/prototype)
Geometric	1 : 15
Elastic modulus	1 : 1
Acceleration	3 : 1
Displacement	1 : 15
Density	5 : 1
Stress	1 : 1
Mass	1 : 130
Time	1 : 6.7
Frequency	6.7 : 1

2.2. Design and Manufacture of the Conductor Line and Ground Line

2.2.1. Similitude Coefficients of the Conductor Line and Ground Line. The tests were carried out using the three-shaking-table array system at Fuzhou University. A 4.1 m × 4.1 m horizontal bidirectional shaking table is in the middle, and two 2.5 m × 2.5 m horizontal bidirectional shaking tables are on each side. The maximum distance between the middle table and the side tables is 10 m, and the horizontal span of the prototype model is 500 m. If the tests are based on a geometric scale ratio of 1 : 15, the dimensions of the shaking tables are unable to meet the requirements. Therefore, in this study, the similitude ratio of the dynamic characteristics and the similitude ratio of the inertial mass are assumed separately to design the similitude coefficients of the conductor lines and ground lines.

(1) Design of the Frequency Similitude Ratio of the Conductor Line and Ground Line. When designing the model of the transmission tower-line coupling system, the similitude ratio of the transmission tower should be close to that of the conductor line and ground line.

The fundamental natural frequency of the conductor line and ground line is as follows:

$$f^{C} = \sqrt{\frac{g}{4\pi^2 s}}, \tag{1}$$

where f^{C} is the fundamental natural frequency of the conductor line and ground line, g is the gravity acceleration constant, and s is the sag in the conductor line and ground line.

The relationship between the frequency similitude ratio and sag similitude ratio of the conductor line and ground line can be derived as follows:

$$S_f = \sqrt{\frac{1}{S_s}}, \qquad S_s = \frac{1}{S_f^2}. \tag{2}$$

The transmission tower has a frequency similitude ratio of 6.7 : 1, and the conductor line and ground line have a frequency similitude ratio of 6.7 : 1 and a sag similitude ratio of 44.9 : 1.

(a) (b)

Figure 2: Counterweights of the test model tower. (a) Counterweight No. 1 (b) Counterweight No. 2.

(2) Design of Mass Similitude Ratio of the Conductor Line and Ground Line. If the geometric similitude ratio of the conductor line and ground line is assumed to be the same as that of the transmission tower (1 : 15), since the span of the prototype tower is 500 m, the distance between the model towers would be 33.33 m, exceeding the maximum distance (10 m) between the middle table and the side table and, hence, not meeting the requirements. Therefore, a span similitude ratio of 1 : 55 is selected for the actual tests, and accordingly, the actual distance between the middle tower and the side tower is 9.09 m.

The mass similitude ratio of the conductor line and ground line is the same as that of the transmission tower (1 : 130). The total mass of the prototype conductor line is $2.06 \times 500 = 1030$ kg, so the mass of the model conductor line is 7.92 kg. The total mass of the prototype ground line is $0.49 \times 500 = 245$ kg. The actual linear densities of the model conductor line and ground line are calculated to be 0.88 kg/m and 0.49 kg/m, respectively (Table 2).

Table 2: Similitude coefficients of the model conductor line and ground line.

Physical quantity	Ratio of similitude (model/prototype)
Actual horizontal span	1 : 55
Theoretical horizontal span	1 : 15
Acceleration	3 : 1
Mass of conductor line	1 : 130
Mass of ground line	1 : 130
Frequency of conductor line	6.7 : 1
Frequency of ground line	6.7 : 1
Elastic modulus of conductor line	1 : 1
Elastic modulus of ground line	1 : 1
Density of conductor line	1 : 2.34
Density of ground line	1 : 2.34

2.2.2. Manufacture of Conductor Line and Ground Line. Steel wires with the diameters of 4 mm and 2 mm are used for the conductor line and ground line, respectively, in the experimental model. The physical components used for the conductor line and ground line are shown in Figure 3.

According to the mass similitude ratio of the conductor line and ground line models, since the density of the steel wire is lower than that of the design model, counterweights are required. The counterweights of the conductor line and ground line are 8 kg and 4 kg, respectively. The counterweight blocks of the corresponding masses are placed uniformly along the conductor line and ground line.

2.3. Design and Manufacture of the Insulator. The V-shaped insulator is simulated by a galvanized plain round steel bar with a diameter of 8 mm and a length of 750 mm, and the I-shaped insulator is simulated by a rigid steel plate with a length of 600 mm and a width of 50 mm. The physical components used for the insulator models are shown in Figure 4. To ensure that the insulator is hinged at two ends with the conductor line, a *U*-shaped steel wire lock is selected to simulate the suspension clamp in the prototype tower, as shown in Figure 5.

2.4. Equivalent Tower. The equivalent tower is the side tower in the three-tower-two-line model and the five-tower-four-line model. The equivalent tower is used to simulate the boundary conditions without considering the similarity relationship with the tower model. In the tests, two equivalent towers are manufactured using welded L50 × 4, as shown in Figure 6. The function of the equivalent tower is similar to that of a corner tower in practical engineering projects.

2.5. Test Models

2.5.1. Single-Tower Model. The test tower is anchored to the rigid base of the shaking table.

2.5.2. Three-Tower-Two-Line Model. The three-tower-two-line model is a single-tower-two-line model that has a cup-type tower as the middle tower and equivalent towers as the side towers. All three towers are anchored to the rigid base of the shaking table. The conductor line and ground line are fixed on the equivalent towers. The boundary conditions are

(a) (b)

Figure 3: Physical components used for the conductor line and ground line. (a) Conductor line (4-mm steel wire). (b) Ground line (2-mm steel wire).

(a) (b)

Figure 4: Physical components used for the insulator models. (a) I-shaped insulator model. (b) V-shaped insulator model.

Figure 5: Physical components used for the conductor line suspension clamp model.

shown in Figure 7, and the physical components used for the three-tower-two-line model are shown in Figure 8.

2.5.3. Five-Tower-Four-Line Model. The five-tower-four-line model is an improved version of the three-tower and two-line model. That is, two new tower models, which are the same as the middle tower, are placed at the locations of the original equivalent towers, which are relocated to the outer side of the new side main towers, along the line direction, and the boundary conditions are simulated through the connection between the equivalent towers and conductor lines, as shown in Figure 9. The physical components used for the five-tower-four-line model are shown in Figure 10.

Figure 6: Equivalent generation tower model.

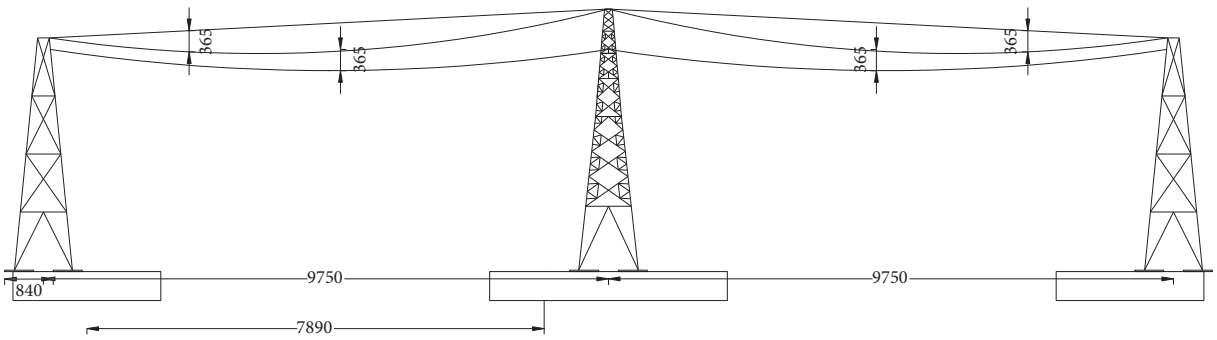

Figure 7: Elevation of the three-tower-two-line model.

Figure 8: Physical components used for the three-tower-two-line model.

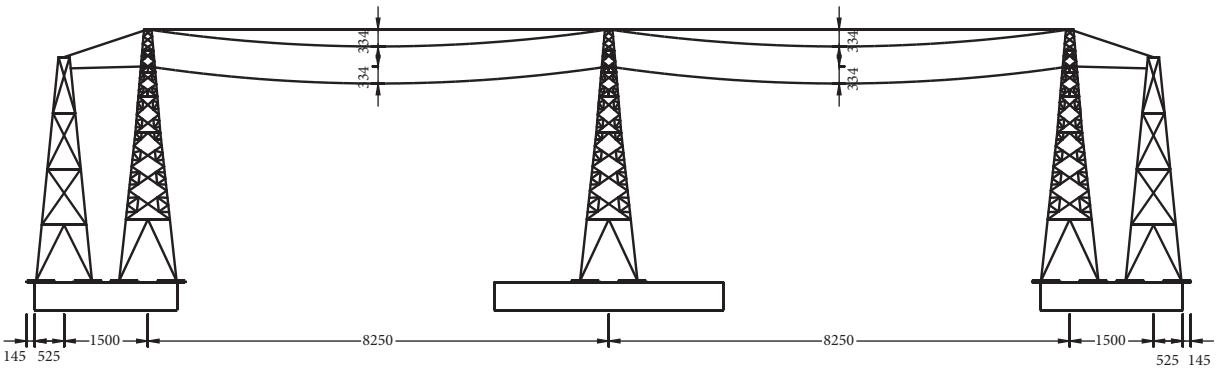

Figure 9: Elevation of the five-tower-four-line model.

3. Shaking Table Test Setup

3.1. Selection of Ground Motions. Considering the long span of transmission lines and the different site conditions in the regions that the lines traverse, the El Centro record, Taft record, and artificial waves are selected for site classes II, III, and IV, respectively. The duration of the ground motion is compressed to 1/6.7 of the original, based on the similarity relationship. The original wave is compressed according to the time or frequency similitude ratio and is then applied to the seismic excitation tests of the scale models. The 0.07 g seismic records are shown in Figure 11.

Figure 10: Physical components used for the five-tower-four-line model.

3.2. Sensor Layout. Two types of acceleration sensors, namely, a piezoresistive accelerometer and piezoelectric accelerometer, are used in the tests. The piezoresistive accelerometer has a large measuring range and is mainly used to measure the seismic responses of the top of the tower and the conductor and ground lines. The piezoelectric accelerometer has a slightly smaller measuring range and is mainly used to measure the seismic responses of the tower leg and body. Two types of displacement sensors, namely, a laser displacement sensor and guyed displacement sensor, are used in the tests. Resistive strain gauges are used in the tests to test the strain of the tower model members.

3.2.1. Sensor Layout for the Single-Tower Model. In the single-tower model tests, a total of 22 acceleration sensors, 25 strain gauges, and 14 displacement sensors are deployed. The detailed placements of the sensors are shown in Figures 12–14, in which "*X*" indicates the longitudinal direction, "*Y*" indicates the transverse direction, as shown by the coordinates in the lower left corner, "*A*" denotes an acceleration sensor, "*S*" denotes a strain gauge, and "*D*" denotes a displacement sensor.

3.2.2. Sensor Layout for the Three-Tower-Two-Line Model

(1) Acceleration Sensors. The layout of the acceleration sensors on the three-tower-two-line model is exactly the same as that on the body of the single-tower model with counterweights. A total of 16 acceleration sensors are deployed on the conductor lines. A total of six acceleration sensors are placed on the ground line. The acceleration sensors are evenly distributed along the conductor and ground lines. The layout of the acceleration sensors on the conductor and ground lines is shown in Figure 15, where *C* represents the acceleration sensor and the numeral represents the numbering of the sensors.

In the "three-tower-two-line" model, four acceleration sensors are placed on each of the two equivalent towers. Specifically, for each equivalent tower, one acceleration sensor is placed in the *X* and *Y* directions on top of the tower, and one acceleration sensor is placed in the *X* and *Y* directions on the base of table. Thus, a total of eight acceleration sensors are placed. The detailed layout is shown in Figure 16, where "*L*" is the left equivalent tower, "*R*" is the right equivalent tower, "*A*" is the acceleration, "*S*" is the strain, "*D*" is the tower top, "*T*" is the tower leg, "*M*" is the table top, and "*X*" and "*Y*" are the two vibration directions. The acceleration sensors are placed at the middle point on the top of the equivalent tower, and the strain gages are placed on the tower legs along the line direction.

(2) Displacement Sensors. The layout of the displacement sensors on the "three-tower-two-line" model is the same as that on the body of the single-tower model with counterweights. Thus, the detailed layout is the layout of the displacement sensors on the single-tower model (Figure 13).

(3) Strain Gauge Layout. The layout of the strain gauges on the "three-tower-two-line" model is the same as that on the body of the single-tower model. The detailed layout is shown in Figure 14, where "*S*" represents a strain gauge and the numeral represents the numbering of the gauges.

3.2.3. Sensor Layout for the Five-Tower-Four-Line Model

(1) Acceleration Sensor. There are three model towers in the "five-tower-four-line" model. Due to the limitations of the sensors and acquisition channels, in particular, 18 acceleration sensors are deployed in the middle tower. The specific layout is illustrated in Figure 17(a), where A represents an acceleration sensor and the numeral represents the numbering of the sensors.

In the five-tower-four-line model, the layout of the sensors on the two model towers on the left and right small tables reference that on the middle tower. A total of 14 acceleration sensors are placed on the right main tower, as shown in Figure 17(b), where *R* represents the right side, A represents an acceleration sensor, and the numeral represents the numbering of the sensors consistent with that of the middle main tower, indicating that the position of a sensor on the side main tower corresponds with that on the middle tower. A total of 11 acceleration sensors are placed on the left main tower, as shown in Figure 17(c), where *L* represents the left side, A represents an acceleration sensor, and the numeral represents the numbering of the sensors consistent with that of the middle main tower, indicating that the position of a sensor on the side main tower corresponds to that on the middle tower.

The layout of the sensors on the equivalent tower in the five-tower-four-line model is identical to that on the equivalent tower of the three-tower-two-line model. The specific layout is illustrated in Figure 16.

A total of three acceleration sensors are deployed on the conductor line, and one acceleration sensor is deployed on the ground line. The specific sensor layout is shown in Figure 18, where *C* represents an acceleration sensor, the numeral represents the numbering of the sensors, and the arrow represents the direction of the vibration.

(2) Displacement Sensors. The layout of the displacement sensors on the towers of the five-tower-four-line model is

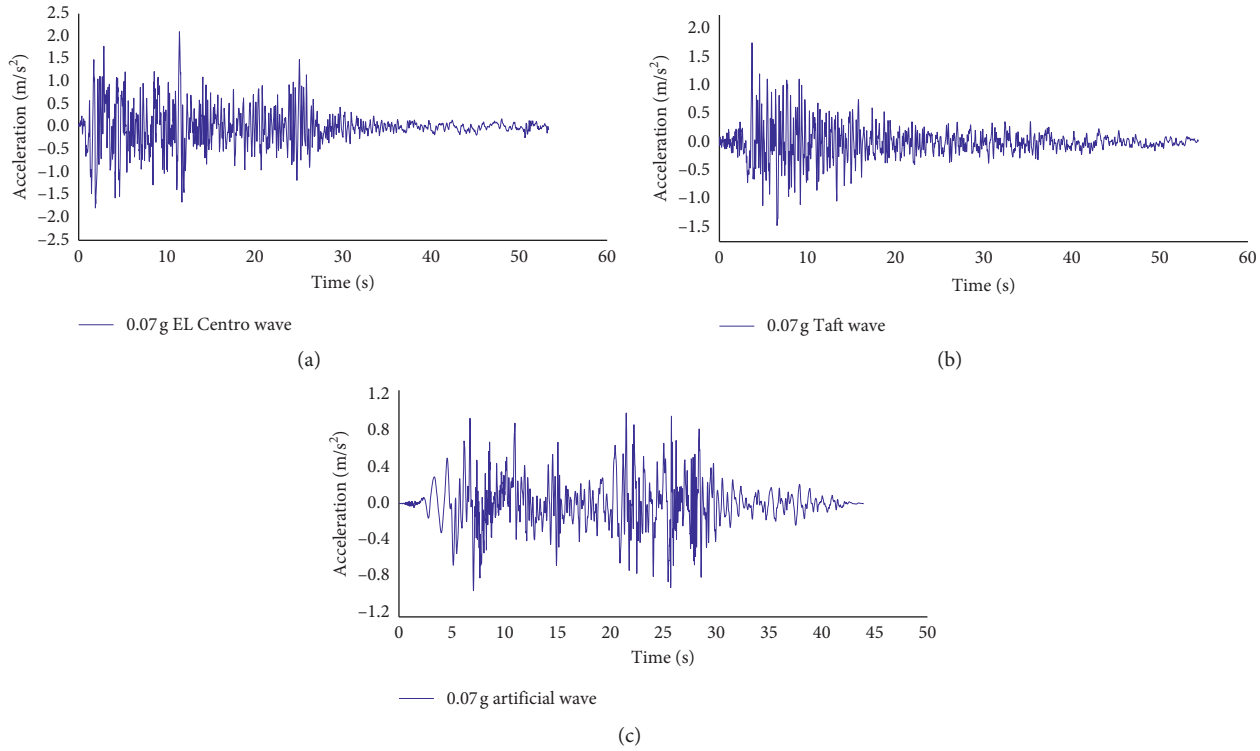

Figure 11: The 0.07 g seismic records. (a) 0.07 g EL Centro wave. (b) 0.07 g Taft wave. (c) 0.07 g artificial wave.

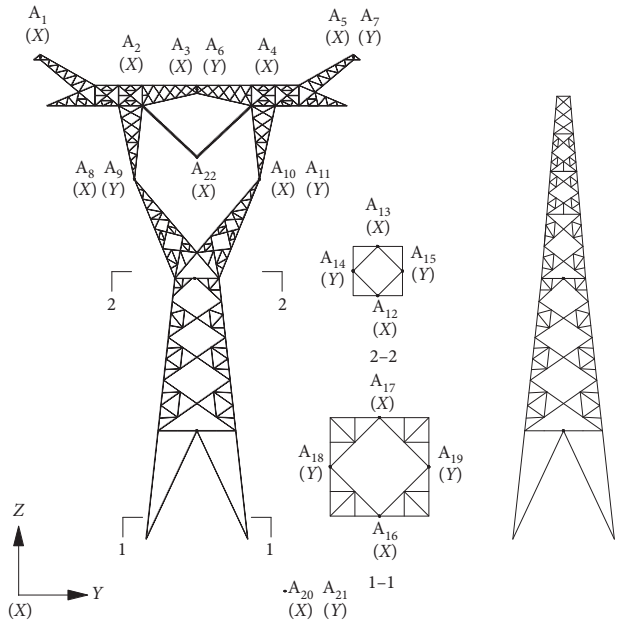

Figure 12: Layout of acceleration sensors.

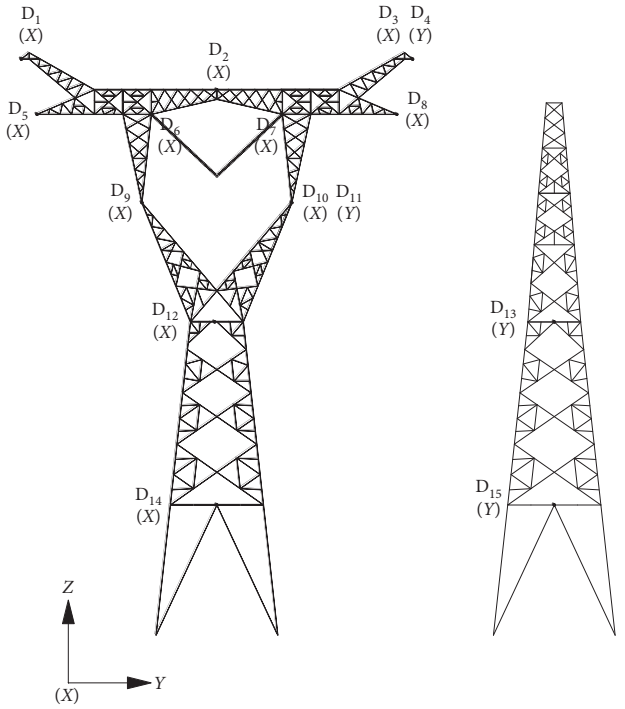

Figure 13: Layout of displacement sensors.

identical to that on the tower of the single-tower model with counterweights. The specific layout references the layout of the displacement sensors on the single-tower model (Figure 13), where D represents the displacement and the numeral represents the numbering of the sensors.

In the five-tower-four-line model, the layouts of the sensors on the two model towers on the left and right small tables reference that on the middle tower, but the sensors are all deployed above the tower structure, where the layout of the sensors above the structure of the right main tower is consistent with that of the middle tower, with 8 displacement

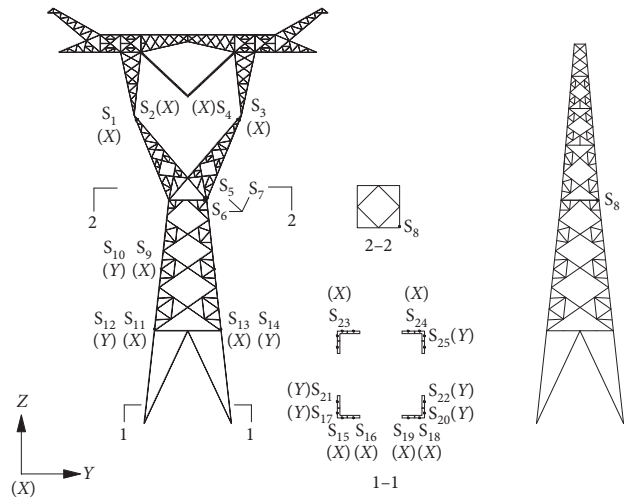

Figure 14: Layout of strain gauges.

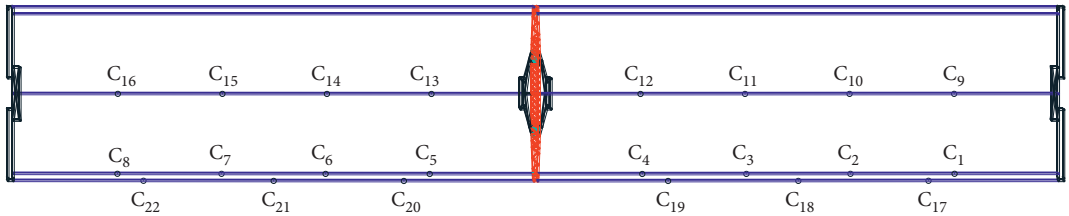

Figure 15: Schematic diagram of the layout of the acceleration sensors on the conductor and ground lines.

sensors placed (Figure 19(a)), while the sensors are symmetrically deployed only on the upper structure of the left main tower, with 4 displacement sensors placed (Figure 19(b)). In the figure, *L* stands for the left side, *R* is the right side, *D* is the displacement sensor, and the numeral is the numbering of the sensors. When the numeral of the main side tower is consistent with that of the middle tower, the location of the sensor on the main side tower corresponds with that on the middle tower. In addition, the direction of the sensor is represented by *X* or *Y*. The specific layout is illustrated in Figure 19.

The five-tower-four-line model has a total of 73 strain gauges, including 28 on the middle tower, 23 on the right main tower, 22 on the left main tower, and 2 on the equivalent tower. Figure 20 illustrates the specific layout of the strain gages.

3.3. Test Program. The basic dynamic characteristics tests and seismic time-history response tests are conducted on the single-tower model, the single-tower model with suspended lumped masses, the three-tower-two-line model, and the five-tower-four-line model. A total of 21 runs were performed, as listed in Table 3.

4. Test Results

To study the influence of the coupling effect of the transmission tower-line system on the transmission tower, dynamic characteristics tests and the shaking table tests are performed on the single-tower model, the single-tower model with suspended lumped masses, the three-tower-two-line model, and the five-tower-four-line model. The results of the frequency, damping, acceleration, displacement, and strain of the middle tower are obtained from the tests.

4.1. Dynamic Characteristics Test Results. Figure 21 shows the spectral analysis results of the acceleration time-history curve at the midpoint of the middle tower model head in the transverse direction (first-order) and the longitudinal direction (second-order) of the four models. Table 4 compares the basic dynamic characteristics of the middle towers of the four models. The results show that the suspension of the conductor lines and lumped masses decreases the frequency of the middle tower. Compared with the single-tower model, the first-order frequency of the single tower with suspended lumped masses model decreases by 5.08%, and the second-order frequency decreases by 4.03%. The frequencies of the two models with suspended conductor lines are very close. Compared with those of the single-tower model, the first-order frequency of the model with suspended conductor lines decreases by 0.82%, and the second-order frequency decreases by 4.0%. In terms of structural damping, the suspension of clumped masses and conductor lines increase the damping ratio of the structure, with the damping ratio of the three-tower-two-line model reaching a maximum of 2.99%. These results show that there is no significant difference regarding the effect of tower-line coupling for the dynamic characteristics between the three-tower-two-line

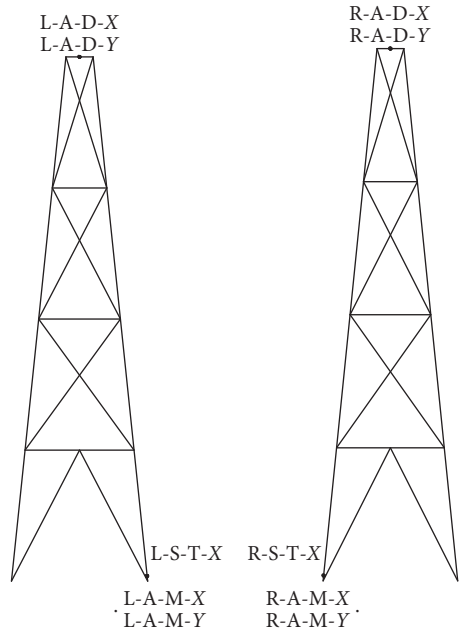

Figure 16: Layout of the accelerator sensors and strain gauges on the equivalent tower model.

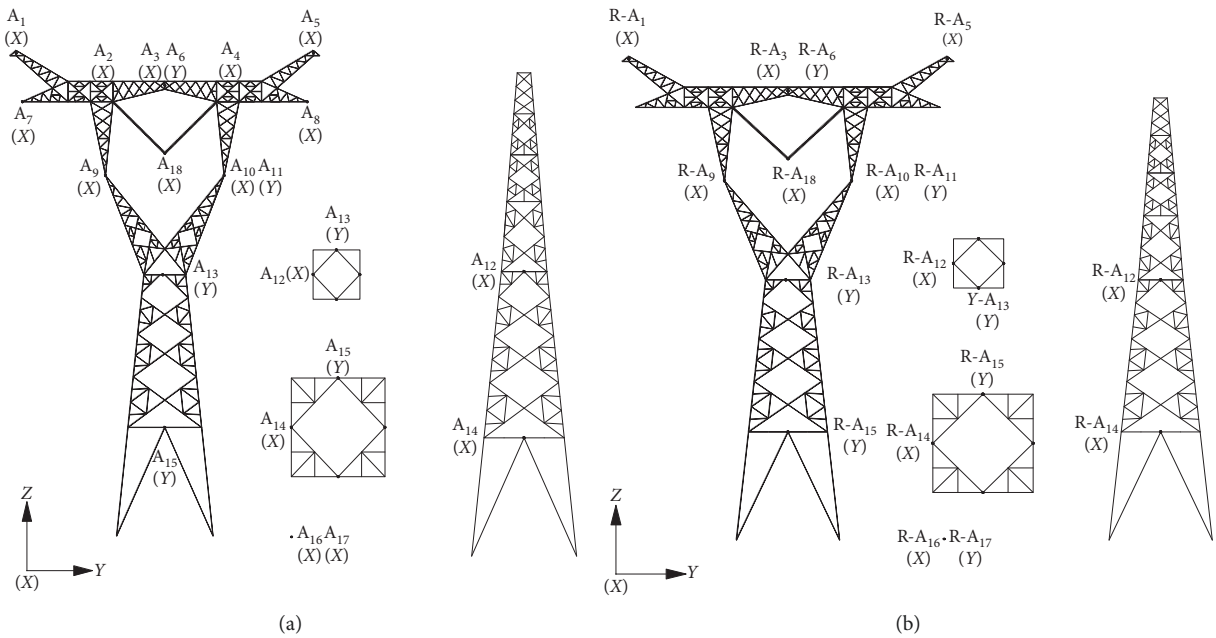

(a) (b)

Figure 17: Continued.

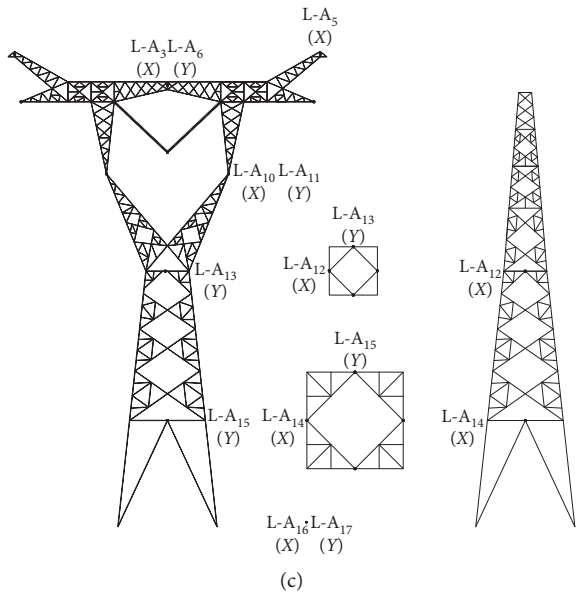

Figure 17: Acceleration sensor placement of the five-tower and four-line model. Layout of the acceleration sensors on (a) the middle tower, (b) the right model tower, and (c) the left model tower.

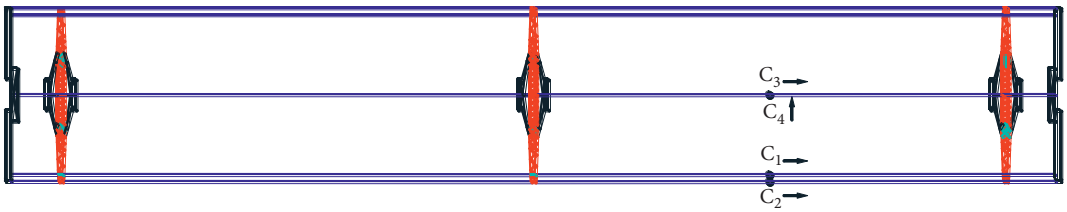

Figure 18: Layout of the acceleration sensors on the five-tower-four-line model.

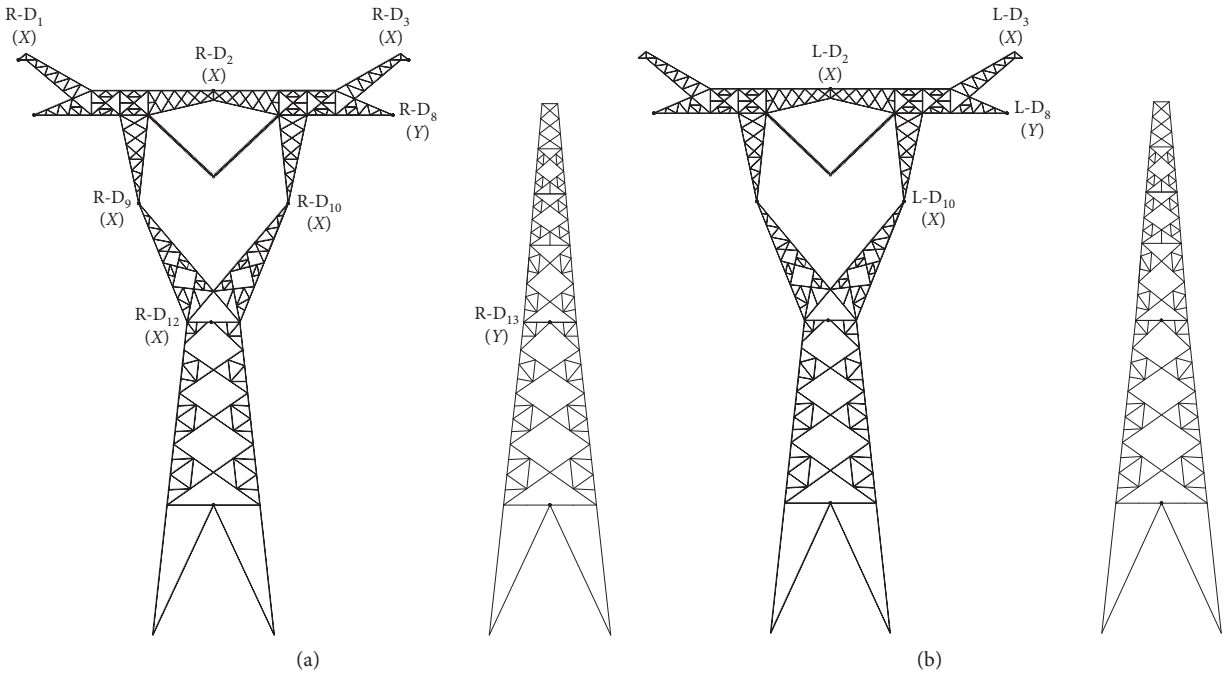

Figure 19: Layout of the displacement sensors on the five-tower-four-line model. Layout of the displacement sensors on (a) the right model tower and (b) the left model tower.

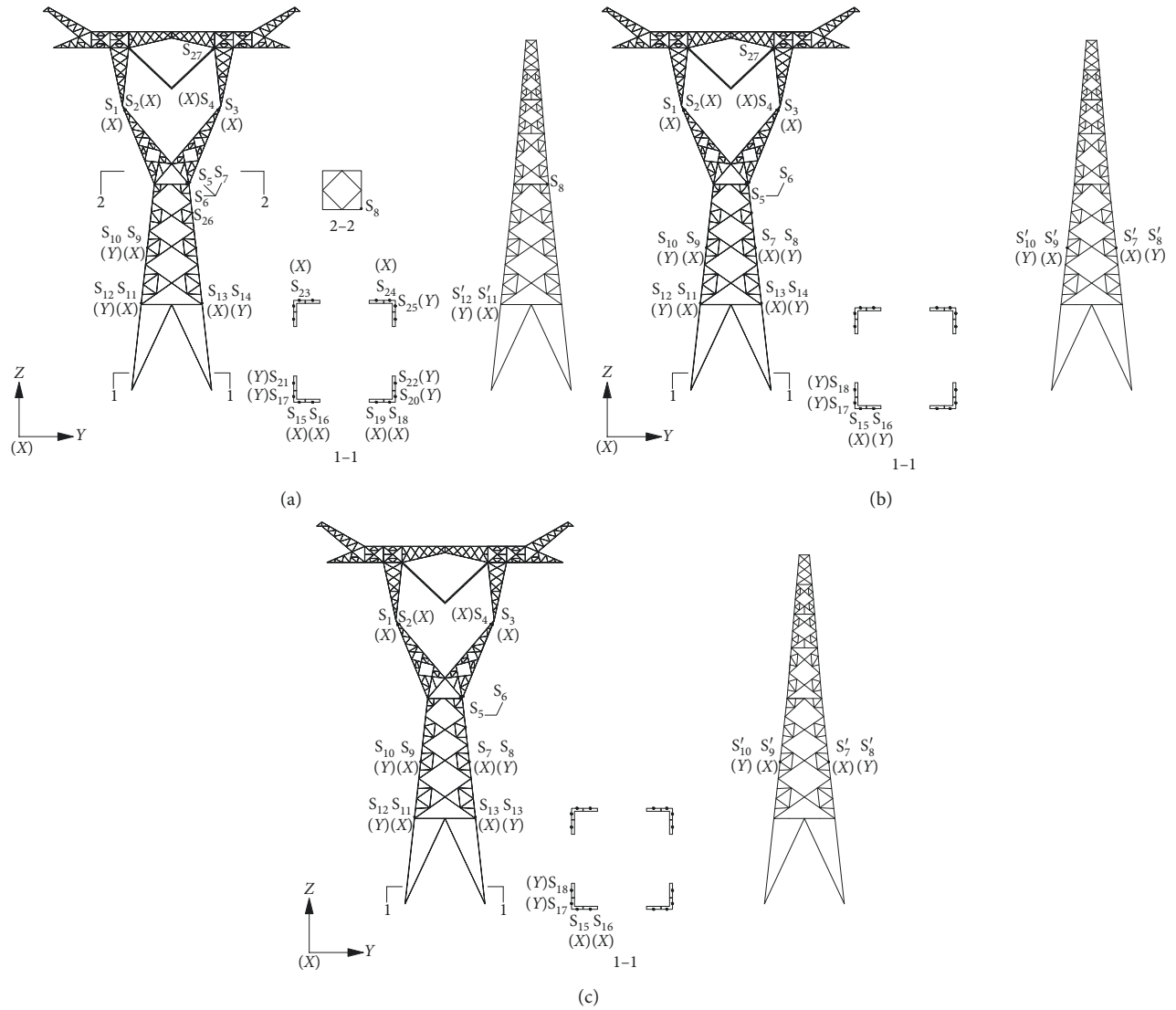

Figure 20: Layout of the strain gauges on the five-tower-four-line model. (a) Layout of 28 strain gauges on the middle tower. (b) Layout of 23 strain gauges on the right main tower. (c) Layout of 22 strain gauges on the left main tower.

model and the five-tower-four-line model. The effect of tower-line coupling decreases the frequency of the tower and increases the damping ratio. The single-tower model with suspended lumped masses can simulate the effect of tower-line coupling on the longitudinal dynamic characteristics of the transmission tower well, but this model faces difficulty in satisfactorily simulating the effect of tower-line coupling on the transverse characteristics of the transmission tower.

4.2. Comparative Analysis of the Dynamic Results of the Middle Towers from the Shaking Table Tests

(1) Comparative Analysis of the Acceleration Response. Figure 22 shows the longitudinal peak acceleration responses under the unidirectional input of a 0.21 g artificial wave. The results show that the peak acceleration response curves of the tower accelerations of the different models basically coincide, and the trends are similar. The peak acceleration response gradually increases from the base of the tower to the top, reaching the maximum at the top of the tower.

Table 5 shows the longitudinal peak acceleration responses of the middle towers of the four models under each wave. The results show that the peak acceleration response is the largest under the artificial wave and the smallest under the El Centro wave. The model with the suspended lumped mass has the smallest acceleration response. Therefore, the use of a single-tower model with suspended lumped masses to simulate a three-tower-two-line model or a five-tower-four-line model is inaccurate. Except for the 0.63 g test condition, the effect of the tower-line coupling increases the longitudinal peak acceleration response of the tower.

Figure 23 shows the transverse peak acceleration response under the unidirectional input of a 0.21 g artificial wave. The results show that except for the single tower with

Table 3: Test program.

Test series	Input wave	Peak acceleration (g)	Loading direction
1	White noise	0.07	—
2	El Centro wave	0.07	*X*
3	Taft wave	0.07	*X*
4	Artificial wave	0.07	*X*
5	El Centro wave	0.07	*Y*
6	Taft wave	0.07	*Y*
7	Artificial wave	0.07	*Y*
8	White noise	0.21	—
9	El Centro wave	0.21	*X*
10	Taft wave	0.21	*X*
11	Artificial wave	0.21	*X*
12	El Centro wave	0.21	*Y*
13	Taft wave	0.21	*Y*
14	Artificial wave	0.21	*Y*
15	White noise	0.63	—
16	El Centro wave	0.63	*X*
17	Taft wave	0.63	*X*
18	Artificial wave	0.63	*X*
19	El Centro wave	0.63	*Y*
20	Taft wave	0.63	*Y*
21	Artificial wave	0.63	*Y*

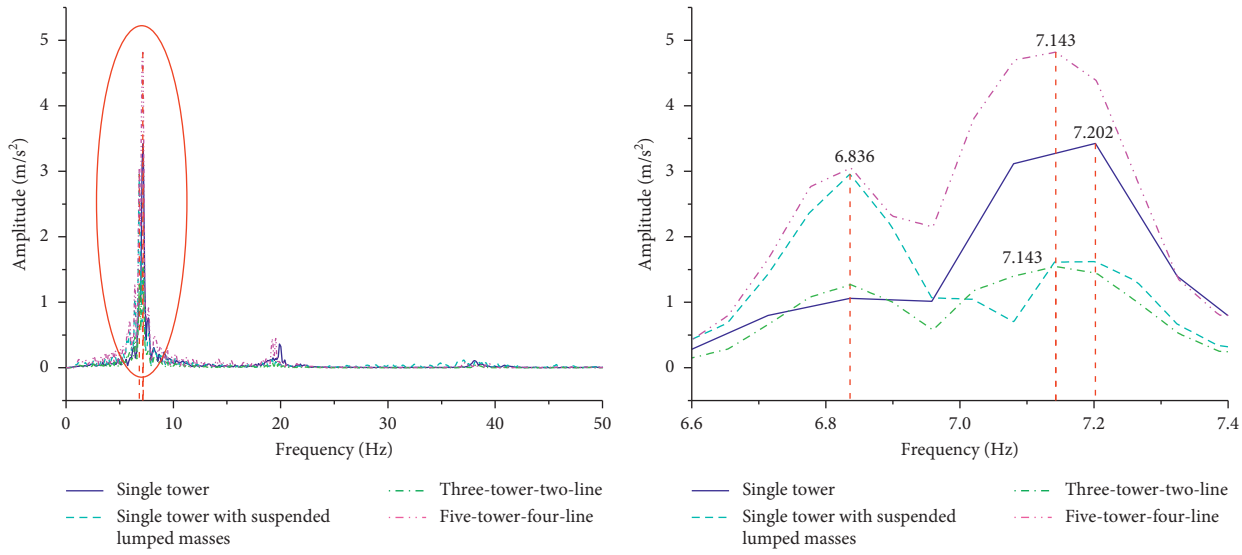

(a)

Figure 21: Continued.

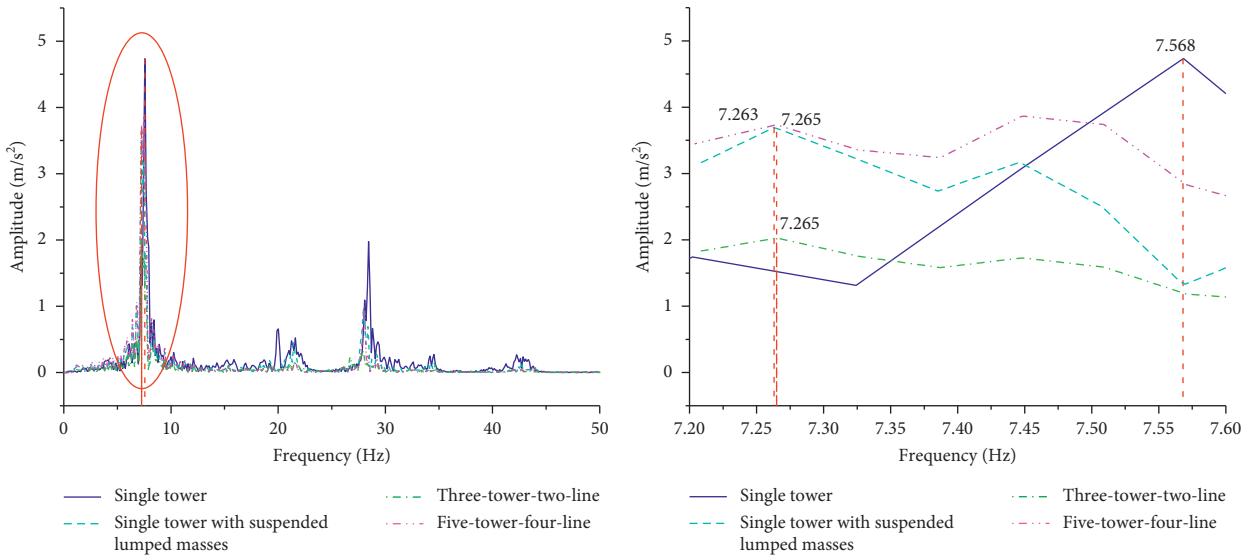

Figure 21: Spectrum analysis curves of the middle towers of the four counterweight models. (a) First-order frequency spectrum analysis curves. (b) Second-order frequency spectrum analysis curves.

Table 4: Comparison of the basic dynamic characteristics of the middle towers of the four models.

Model	Frequency		Damping ratio	
	$f1$ (Hz)	$f2$ (Hz)	$C1$ (%)	$C2$ (%)
Single-tower model	7.202	7.568	0.92	2.40
Single tower with suspended lumped masses	6.836	7.263	1.06	1.18
Three-tower-two-line model	7.143	7.265	2.99	2.58
Five-tower-four-line model	7.143	7.265	2.38	1.65

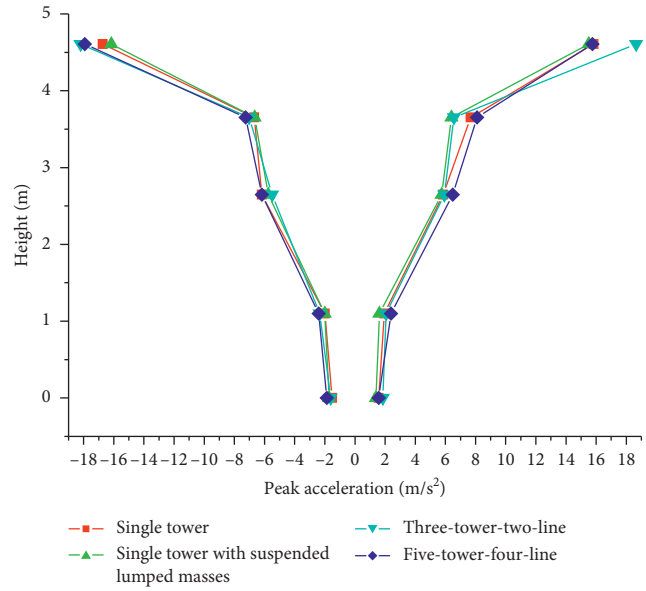

Figure 22: Longitudinal peak acceleration responses of the middle tower of the four models under a 0.21 g artificial wave.

suspended lumped masses model, the peak acceleration response curves of the towers of the other models basically coincide and have similar trends. The comparison shows that the peak accelerations are relatively close within the lower portion of the tower structure, while the peak acceleration responses at the crossarm vary noticeably. The

Table 5: Longitudinal peak acceleration responses of the middle towers of the four models.

Test series	Single-tower model (m/s^2)	Single-tower model with suspended lumped masses (m/s^2)	Three-tower-two-line model (m/s^2)	Five-tower-four-line model (m/s^2)
0.07 g artificial wave	5.966	5.278	5.905	7.310
0.07 g El Centro wave	4.563	4.122	4.456	4.096
0.07 g Taft wave	5.137	4.202	5.961	5.810
0.07 g average	5.222	4.534	5.441	5.739
0.21 g artificial wave	16.738	16.166	18.663	17.921
0.21 g El Centro wave	14.291	11.379	16.815	11.809
0.21 g Taft wave	15.791	13.880	17.458	16.866
0.21 g average	15.607	13.808	17.646	15.532
0.63 g artificial wave	64.671	41.566	46.214	57.260
0.63 g El Centro wave	46.165	36.703	45.403	38.731
0.63 g Taft wave	53.828	41.161	41.546	49.032
0.63 g average	54.888	39.810	44.388	48.341

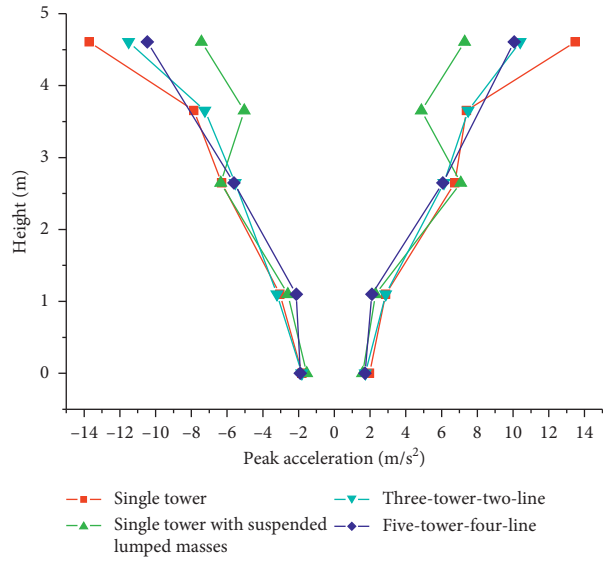

Figure 23: Transverse peak acceleration responses of the four counterweight models under a 0.21 g artificial wave.

Table 6: Vertical peak acceleration responses of the middle towers of the four models.

Test series	Single-tower model (m/s^2)	Single-tower model with suspended lumped masses (m/s^2)	Three-tower-two-line model (m/s^2)	Five-tower-four-line model (m/s^2)
0.07 g artificial wave	4.612	2.563	3.662	4.059
0.07 g El Centro wave	1.795	1.192	1.716	1.538
0.07 g Taft wave	3.349	2.236	2.996	2.333
0.07 g average	3.252	1.997	2.791	2.643
0.21 g artificial wave	13.710	7.441	11.511	10.878
0.21 g El Centro wave	5.827	4.911	5.669	4.603
0.21 g Taft wave	10.963	6.676	9.522	7.003
0.21 g average	10.167	6.343	8.901	7.495
0.63 g artificial wave	35.349	21.697	32.248	26.287
0.63 g El Centro wave	17.258	13.433	18.088	13.516
0.63 g Taft wave	29.543	20.806	24.010	20.001
0.63 g average	27.383	18.645	24.782	19.935

peak acceleration of the single-tower model with suspended lumped masses is the smallest at the crossarm, and the peak acceleration of the single-tower model is the largest at the crossarm.

Table 6 shows the transverse peak accelerations of the middle towers of the four models under each wave. The results show that the peak acceleration response is the largest under the artificial wave and is the smallest under the El

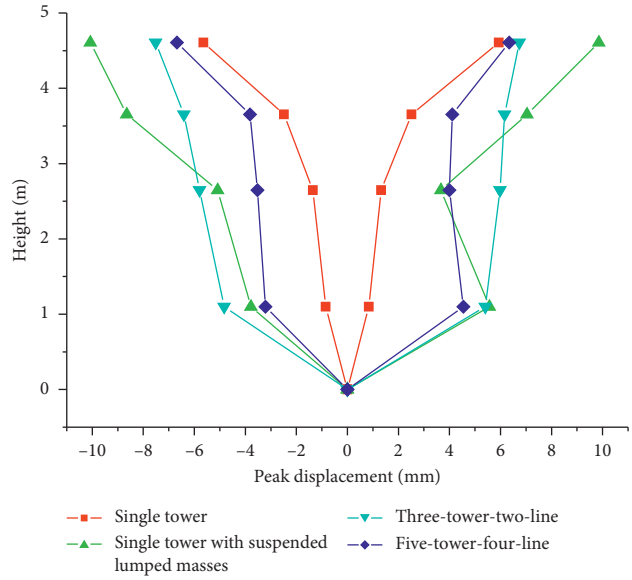

Figure 24: Longitudinal peak displacement responses of the four models under a 0.21 g artificial wave.

Table 7: Longitudinal peak displacement responses of the middle towers of the four models.

Test series	Single-tower model (mm)	Single-tower model with suspended lumped masses (mm)	Three-tower-consistency model (mm)	Five-tower-consistency model (mm)
0.07 g artificial wave	1.737	2.963	2.456	2.021
0.07 g El Centro wave	0.989	0.979	1.389	1.329
0.07 g Taft wave	1.161	1.474	1.149	1.304
0.07 g average	1.296	1.805	1.665	1.551
0.21 g artificial wave	5.936	10.072	7.516	6.681
0.21 g El Centro wave	4.155	6.321	4.876	3.799
0.21 g Taft wave	3.619	5.076	3.710	4.593
0.21 g average	4.570	7.156	5.368	5.024
0.63 g artificial wave	30.041	35.823	27.151	19.555
0.63 g El Centro wave	15.137	22.200	14.378	12.541
0.63 g Taft wave	14.462	15.054	10.921	13.204
0.63 g average	19.880	24.359	17.483	15.100

Centro wave. The model with suspended lumped masses has the lowest peak acceleration response, and the single-tower model with counterweights has the highest peak acceleration response. Therefore, the suspended masses and conductor lines are decreasing the transverse seismic response of the model tower. In comparison, the single tower with suspended lumped masses tested using a single shaking table has the lowest seismic response, so the use of this model to simulate the tower-line system is inaccurate. Under the three seismic conditions of the same seismic intensity level, the average transverse peak acceleration response of the three-tower-two-line model is greater than that of the five-tower-four-line model; the effect of tower-line coupling decreases the transverse peak acceleration response of the tower.

(2) Comparative Analysis of the Displacement Responses. Figure 24 shows the longitudinal peak displacement responses under the unidirectional input of a 0.21 g artificial wave. The results show that except for that of the single-tower model with suspended lumped masses, the peak displacement response gradually increases from the base of the tower to the top, reaching the maximum peak displacement at the top of the tower.

Table 7 shows the longitudinal peak displacements of the main towers of the four models under each wave. The results show that the peak displacement response is the largest under the artificial wave and is the smallest under the El Centro wave. The single-tower model with suspended lumped masses has the maximum displacement response. Under the three test conditions at the same seismic level, the average of the longitudinal peak displacement responses of the three-tower-consistency model is larger than that of the five-tower-consistency model. Except for 0.63 g test condition, the effect of tower-line coupling increases the longitudinal peak displacement response of the tower.

Figure 25 shows the transverse peak displacement responses under the unidirectional input of a 0.21 g artificial wave. The results show that the trends of the peak displacement response curves of the towers are similar. The peak displacement response gradually increases from

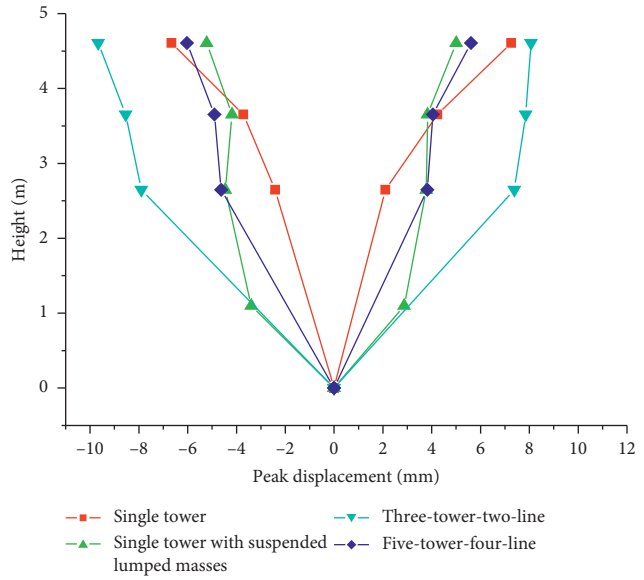

Figure 25: Transverse peak displacement responses of the four models under a 0.21 g artificial wave.

Table 8: Transverse peak displacement responses of the middle towers of the four models.

Test series	Single-tower model (mm)	Single-tower model with suspended lumped masses (mm)	Three-tower-two-line model (mm)	Five-tower-four-line model (mm)
0.07 g artificial wave	2.134	1.687	3.126	1.848
0.07 g El Centro wave	0.811	0.543	0.720	0.736
0.07 g Taft wave	1.127	0.883	0.824	0.897
0.07 g average	1.357	1.038	1.557	1.161
0.21 g artificial wave	7.258	5.223	9.663	6.032
0.21 g El Centro wave	2.148	2.447	2.514	2.089
0.21 g Taft wave	3.962	2.233	2.976	3.130
0.21 g average	4.456	3.301	5.051	3.750
0.63 g artificial wave	21.152	16.141	26.785	16.364
0.63 g El Centro wave	7.513	7.250	8.162	6.549
0.63 g Taft wave	12.204	7.045	7.768	8.783
0.63 g average	13.623	10.146	14.238	10.565

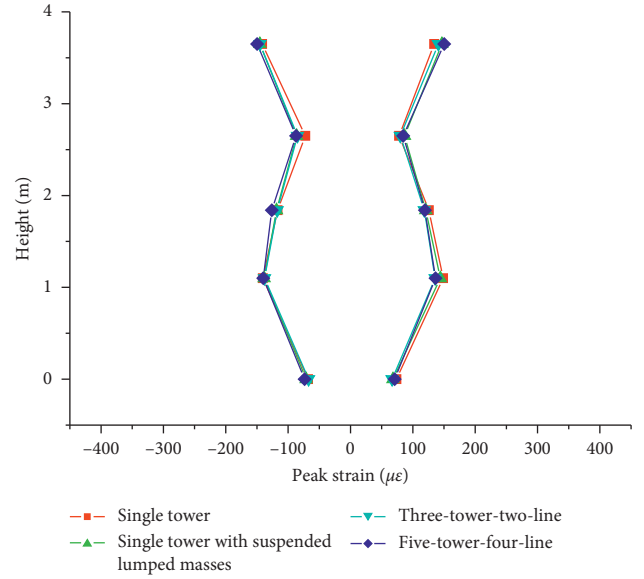

Figure 26: Longitudinal peak strain responses of the four models under a 0.21 g artificial wave.

Table 9: Longitudinal peak strain responses of the middle towers of the four models.

Test series	Single-tower model ($\mu\varepsilon$)	Single-tower model with suspended lumped masses ($\mu\varepsilon$)	Three-tower-two-line model ($\mu\varepsilon$)	Five-tower-four-line model ($\mu\varepsilon$)
0.07 g artificial wave	53.546	59.655	56.044	56.169
0.07 g El Centro wave	28.017	33.378	33.323	33.819
0.07 g Taft wave	33.187	37.373	33.432	34.995
0.07 g average	38.250	43.469	40.933	41.661
0.21 g artificial wave	148.616	171.750	167.730	150.257
0.21 g El Centro wave	101.668	108.935	129.404	104.848
0.21 g Taft wave	106.910	117.344	111.988	122.553
0.21 g average	119.065	132.677	136.374	125.886
0.63 g artificial wave	450.086	426.452	442.957	513.300
0.63 g El Centro wave	358.235	359.335	394.204	347.420
0.63 g Taft wave	394.345	347.076	306.438	377.690
0.63 g average	400.888	377.621	381.200	412.803

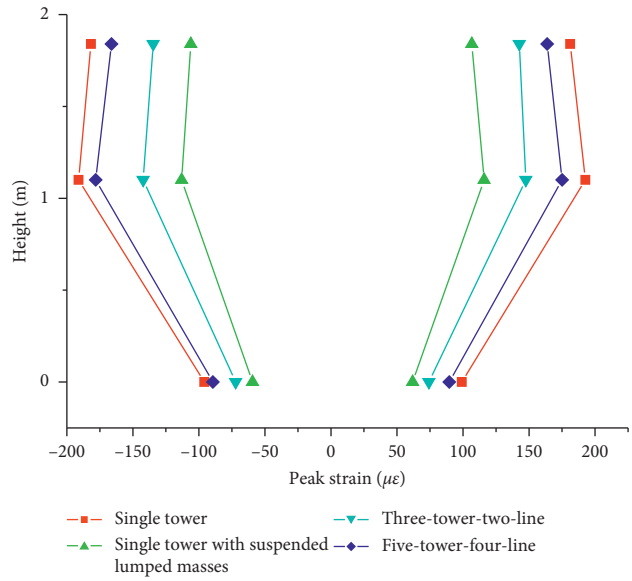

Figure 27: Transverse peak strain responses of the four counterweight models under a 0.21 g artificial wave.

the base of the tower to the top, reaching the largest peak displacement at the top of the tower.

Table 8 shows the transverse peak displacements of the main towers of the four models under each wave. The results show that the peak displacement response is the largest under the artificial wave and is the smallest under the El Centro wave. The single-tower model with suspended lumped masses has the smallest peak displacement response, and the three-tower-two-line model has the largest peak displacement response. Therefore, the use of the single-tower model with suspended lumped masses to simulate the tower-line system is inaccurate. Under the three test conditions at the same seismic level, the average of the transverse peak displacement response of the three-tower-two-line model is larger than that of the five-tower-four-line model; the effect of the three-tower-two-line model's tower-line coupling increases the transverse peak displacement response of the tower, while the effect of the five-tower-four-line model's tower-line coupling decreases the transverse peak displacement response of the tower.

(3) Comparative Analysis of the Strain Responses. Figure 26 shows that for the four models under a 0.21 g unidirectional seismic input, the longitudinal peak strain variation curves of the towers under the crank arms are consistent in both shape and magnitude, and the strain is relatively large at the locations of the tower head, crank arm, and tower legs.

Table 9 shows the longitudinal peak strain values of the main tower strains of the four models under each wave. The results show that the peak strain response is the largest under the artificial wave and is the smallest under the El Centro wave. The longitudinal peak strains of the main towers of the four models are relatively close under the same wave. Except for the 0.63 g test condition, the effect of tower-line coupling increases the longitudinal peak strain response of the tower.

Figure 27 shows the curves of the transverse peak strain values of the tower body structure for the four models under a 0.21 g unidirectional seismic input. The curves are consistent in shape, with parallel decreasing trends. The largest peak strain occurs in the single-tower model, reaching approximately 200 $\mu\varepsilon$, and the smallest peak strain occurs in

Table 10: Transverse peak strain responses of the middle towers of the four models.

Test series	Single-tower model ($\mu\varepsilon$)	Single-tower model with suspended lumped masses ($\mu\varepsilon$)	Three-tower-two-line model ($\mu\varepsilon$)	Five towers and four lines ($\mu\varepsilon$)
0.07 g artificial wave	60.648	40.017	58.052	57.997
0.07 g El Centro wave	19.677	17.108	23.169	19.698
0.07 g Taft wave	37.271	30.922	35.836	41.472
0.07 g average	39.199	29.349	39.019	39.722
0.21 g artificial wave	192.680	115.984	147.565	178.187
0.21 g El Centro wave	65.084	62.486	65.149	64.533
0.21 g Taft wave	129.431	88.464	110.259	118.373
0.21 g average	129.065	88.978	107.658	120.364
0.63 g artificial wave	573.068	359.498	410.263	469.876
0.63 g El Centro wave	193.587	174.849	178.199	197.560
0.63 g Taft wave	384.188	253.697	298.134	351.734
0.63 g average	383.614	262.681	295.532	339.723

the single-tower model with suspended lumped masses, which is approximately 1/2 of that of single-tower model without suspended lumped masses.

Table 10 shows the transverse peak strain values of the main tower of the four models under each wave. The results show that the peak strain response is the largest under the artificial wave and the smallest under the El Centro wave. Except for the 0.21-g test condition, the model with suspended lumped masses has the smallest peak strain response, and the single-tower model has the largest peak strain response. Therefore, the suspended masses and conductor lines reduce the transverse seismic response of the model tower. The effect of tower-line coupling decreases the transverse peak strain response of the tower.

5. Conclusions

In this study, three-shaking-table array system tests of UHV cup-type transmission tower-line systems were carried out, and the dynamic characteristics and seismic responses of a single-tower model, a single-tower model with suspended lumped masses, a three-tower-two-line model, and a five-tower-four-line model were studied. The test results demonstrated the following:

(1) The suspended conductor lines and suspended lumped masses reduce the frequency of the middle tower. The single-tower model with suspended lumped masses can simulate the effect of tower-line coupling on the longitudinal dynamic characteristics of the transmission tower well but cannot simulate the transverse dynamic characteristics of the transmission tower. The dynamic characteristics of the three-tower-two-line model are very close to those of the five-tower-four-line model. The effect of tower-line coupling decreased the frequency of the tower but increased the damping ratio.

(2) Under longitudinal ground motion, except for the single-tower model with suspended lumped masses, the peak accelerations and peak displacements of the other models gradually increase from the base of the tower to the top, reaching the highest peak acceleration and peak displacement at the top of the tower. The peak strain curves of the four models below the crank arm are consistent in shape and magnitude, and the strains are relatively large at the tower head, crank arms, and tower legs. The model with suspended lumped masses has the lowest peak acceleration response and the largest peak displacement response. The longitudinal peak strains of the main towers of the four models under waves are relatively close. Except for 0.63 g seismic condition, the effect of tower-line coupling increased the longitudinal peak acceleration, displacement, and strain response of the tower.

(3) Under transverse ground motion, except for the single-tower model with suspended lumped masses, the peak acceleration responses and peak displacements of the other models gradually increase from the base of the tower to the top, reaching the highest peak acceleration and peak displacement values at the top of the tower. The transverse peak strain curves of the tower structure are consistent in shape, with a parallel decreasing trend, and the model with counterweights has the largest peak strain. The model with suspended lumped masses has the smallest transverse peak acceleration responses for acceleration, displacement, and strain, and use of this model to simulate the tower-line system is inaccurate. Under the three seismic conditions of the same seismic intensity level, the effect of tower-line coupling decreases the transverse peak acceleration response of the tower, the effect of the three-tower-two-line model's tower-line coupling increases the transverse peak displacement response of the tower, while the effect of the five-tower-four-line model's tower-line coupling decreases the transverse peak displacement response of the tower. Except for 0.21 g seismic condition, the effect of tower-line coupling decreased the transverse peak strain response of the tower.

Data Availability

The data used to support the findings of this study are included within the article.

Conflicts of Interest

The authors declare that there are no conflicts of interest regarding the publication of this paper.

Acknowledgments

This study was supported by a fund from the Scientific Research Fund of the Institute of Engineering Mechanics, CEA (Nos. 2019B05 and 2019C10), the National Natural Science Foundation of China (Nos. 51878631 and 51608287), and the National Key Research and Development Program of China (Nos. 2017YFC1500605 and 2018YFC1504602-01).

References

[1] L. Tian, R. S. Ma, F. Zhu et al., "Seismic research progress of high voltage transmission tower-line system," *World Earthquake Engineering*, vol. 30, no. 1, pp. 87–95, 2014.

[2] H. N. Li and H. F. Bai, "State-of-the-art review on studies of disaster resistance of high-voltage transmission tower-line systems," *China Civil Engineering Journal*, vol. 40, no. 2, pp. 39–46, 2007, in Chinese.

[3] L. Tian, W. F. Li, and Z. L. Wang, "Study on suspended mass pendulums for vibration control of transmission tower under seismic excitation," *Advanced Materials Research*, vol. 446–449, pp. 3323–3327, 2012.

[4] H.-N. Li, W.-L. Shi, G.-X. Wang, and L.-G. Jia, "Simplified models and experimental verification for coupled transmission tower-line system to seismic excitations," *Journal of Sound and Vibration*, vol. 286, no. 3, pp. 569–585, 2005.

[5] S. C. Yang and H. P. Hong, "Nonlinear inelastic responses of transmission tower-line system under downburst wind," *Engineering Structures*, vol. 123, no. 15, pp. 490–500, 2016.

[6] F. Yang, H. Dang, H. Niu, H. Zhang, and B. Zhu, "Wind tunnel tests on wind loads acting on an angled steel triangular transmission tower," *Journal of Wind Engineering and Industrial Aerodynamics*, vol. 156, pp. 93–103, 2016.

[7] F. L. Yang, H. J. Zhang, J. B. Yang, H. X. Dang, and J. J. Liu, "Bearing capacity analysis and load values of transmission towers under thunderstorm downburst," *Proceedings of the CSEE*, vol. 34, no. 24, pp. 4179–4186, 2014, in Chinese.

[8] W. J. Lou, X. Liang, Y. Jiang, X. H. Jin, and Z. H. Wang, "Wind-induced response and wind load factor of transmission tower under terrain B wind field and typhoon wind field," *Journal of Vibration and Shock*, vol. 32, no. 6, pp. 13–17, 2013.

[9] J. Li, Q. Yan, Q. Xie, and J. Chen, "Wind field measurements and wind-induced vibration responses of transmission tower during typhoon wipha," *Journal of Architecture and Civil Engineering*, vol. 26, no. 2, pp. 1–8, 2009.

[10] Z. Yan, B. Z. Zhu, X. F. Zi, and Y. X. Xi, "Seismic response analysis of tower-foundation-soil dynamic interaction in transmission line engineering," *Advanced Materials Research*, vol. 1065–1069, pp. 1112–1116, 2014.

[11] Q. Xie, "State-of-the-art of seismic disaster research and emergency response of electric power system," *Electric Power Construction*, vol. 29, no. 8, pp. 2–6, 2008.

[12] Z. Y. Zhang, B. Zhao, W. W. Cao, Y. Li, and Z. X. Ge, "Investigation and preliminary analysis of damages on the power grid in the wenchuan earthquake of M8.0," *Electric Power Technologic Economics*, vol. 20, no. 4, pp. 1–4, 2008.

[13] H. B. You and F. X. Zhao, "M7.0 earthquake in lushan and damage cause analysis of power facilities," *Electric Power Construction*, vol. 34, no. 8, pp. 100–104, 2013, in Chinese.

[14] Z. Xu, W. M. Wang, Q. H. Lin et al., "Progressive collapse analysis of a simplified model for transmission tower-line coupled system under seismic action," *China Earthquake Engineering Journal*, vol. 7, no. 2, pp. 304–309, 2015, in Chinese.

[15] Q. H. Lin, W. M. Wang, D. J. Cao, S. Jin, L. Tian, and L. Wang, "Progressive collapse analysis of high-voltage transmission tower under earthquake action," *Sichuan Building Science*, vol. 40, no. 3, pp. 157–161, 2014.

[16] S. Kotsubo, T. Takanishi, and T. Sonoda, "Dynamic tests and seismic analysis of high towers of electrical transmission line," *Transactions of the Japan Society of Civil Engineers*, vol. 15, pp. 72–75, 1985.

[17] A. Filiatrault and C. Stearns, "Seismic response of electrical substation equipment interconnected by flexible conductors," *Journal of Structural Engineering*, vol. 130, no. 5, pp. 769–778, 2004.

[18] J. L. Kempner and R. C. Stroud, "Transmission line dynamic/static structural testing," *Journal of the Structural Division*, vol. 107, no. 10, pp. 1895–1906, 1981.

[19] L. Tian, H. N. Li, and L. Z. Huang, "Non-proportional problem in shaking table model of a power transmission tower-line system," *Journal of Vibration and Shock*, vol. 31, no. 6, pp. 114–118, 2012, in Chinese.

[20] W. L. Shi, L. H. Nan, and J. L. Guang, "Shaking table test of coupled system of transmission lines and towers," *Engineering Mechanics*, vol. 23, no. 5, pp. 89–93, 2006, in Chinese.

[21] J. Bai, Q. Xie, and S. T. Xue, "Design theory and method of shaking table test model for a UHV double circuit transmission tower-line coupled system," *Journal of Vibration and Shock*, vol. 32, no. 22, pp. 47–52, 2013.

[22] J. Bai, Q. Xie, S. T. Xue, and D. M. Shen, "Shaking table test model design for UHV latticed transmission tower-line coupling system," *Journal of Hunan University (Natural Science Edition)*, vol. 40, no. 4, pp. 20–25, 2013.

[23] Q. Xie, J. Bai, S. T. Xue, and Q. Q. Zhi, "Shaking table test on nonlinear vibration responses of UHV transmission tower-line coupling system," *Earthquake Engineering and Engineering Vibration*, vol. 32, no. 5, pp. 103–110, 2012.

[24] Q. Xie, J. Bai, S. T. Xue, and Q. Q. Zhi, "Shaking table test on 1000 kV angle steel transmission tower," *Power System Technology*, vol. 37, no. 1, pp. 58–64, 2013, in Chinese.

[25] J. Bai, Q. Xie, and S. T. Xue, "Shaking table tests on 1000 kV UHV AC double circuit transmission tower-conductor coupling systems," *Proceedings of the CSEE*, vol. 33, no. 7, pp. 116–123, 2013.